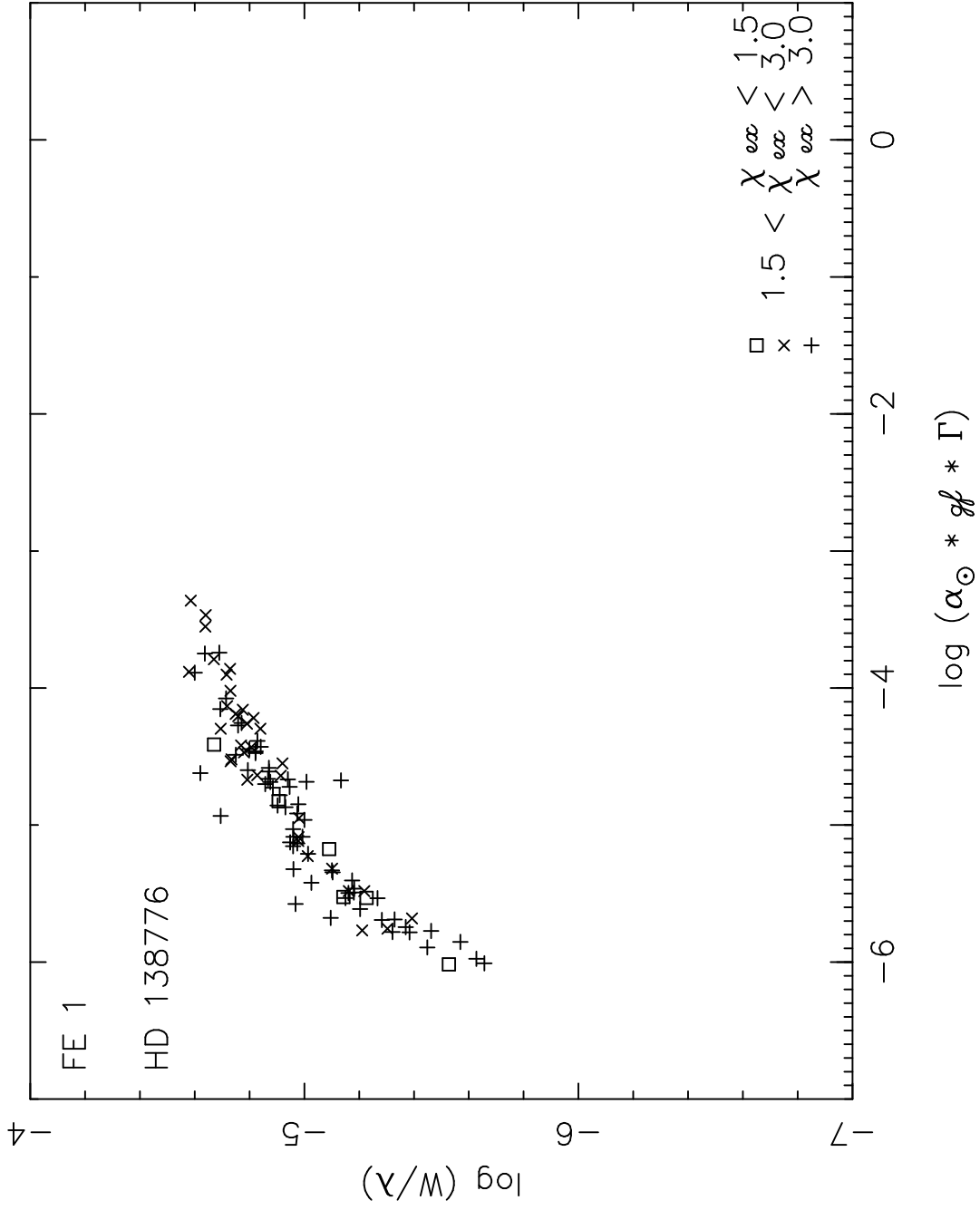
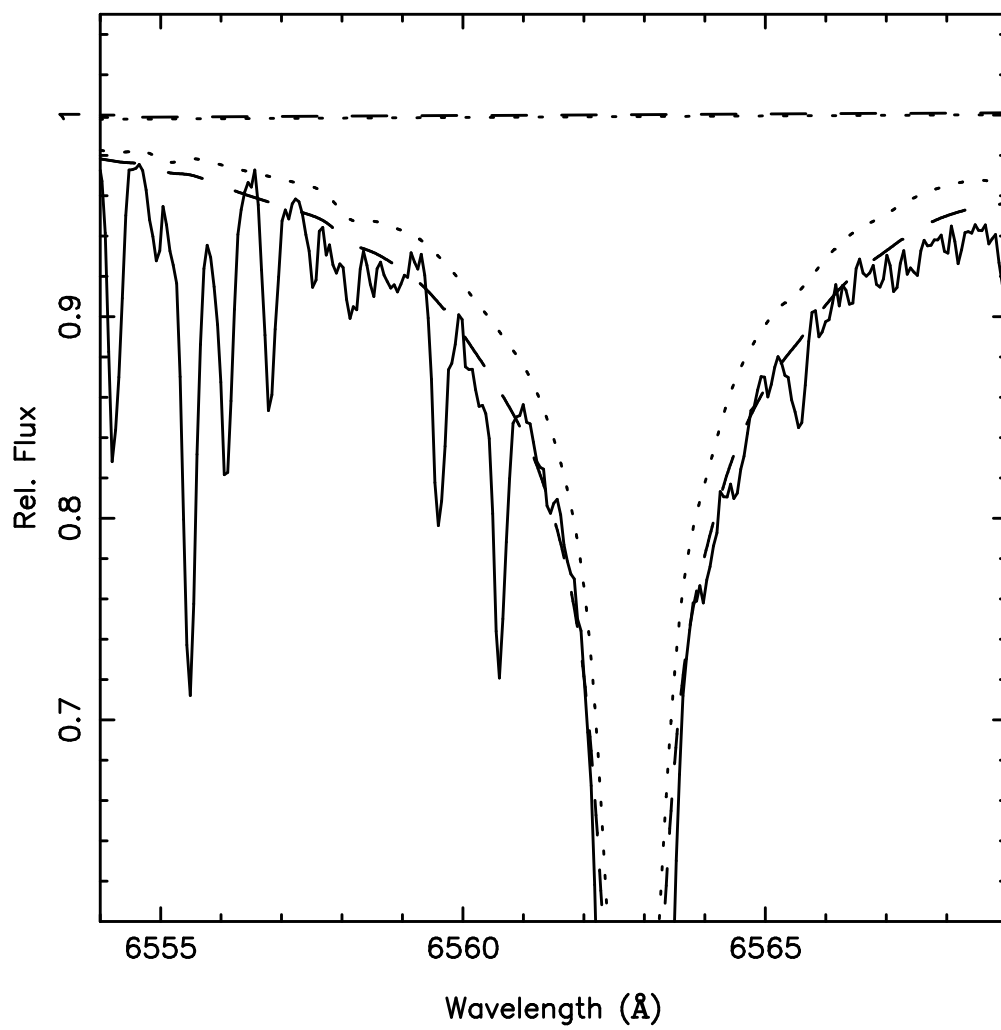


TABLE 1. LOG-BOOK OF OBSERVATIONS

star	V	v_r (km.s $^{-1}$)	α_{1950}	δ_{1950}	Date	exp. time(m)	S/N
BD + 9°1617	9.2	+37.9	07 17 09	09 19.7	3.07.93	30	105
BD - 10°3166	10.0	+25.8	10 55 59	-10 30.1	3.07.93	30	75
BD - 11°4126	10.4	-47.7	16 20 40	-11 28.7	3.08.93	30	80
G161 - 29	11.3	+32.5	09 23 13	-06 33.1	3.08.93	40	60
G60 - 6	11.1	-26.2	12 25 29	07 43.8	3.08.93	45	65
HD 99109	9.1	+28.5	11 21 44	-01 15.1	3.08.93	10	90
HD 115589	9.6	-38.4	13 15 35	-14 19.1	3.07.93	30	105
HD 126614	8.8	-55.0	14 24 12	-04 57.1	3.07.93	30	85
HD 138776	8.7	-17.2	15 31 41	-0233.3	3.07.93	10	90





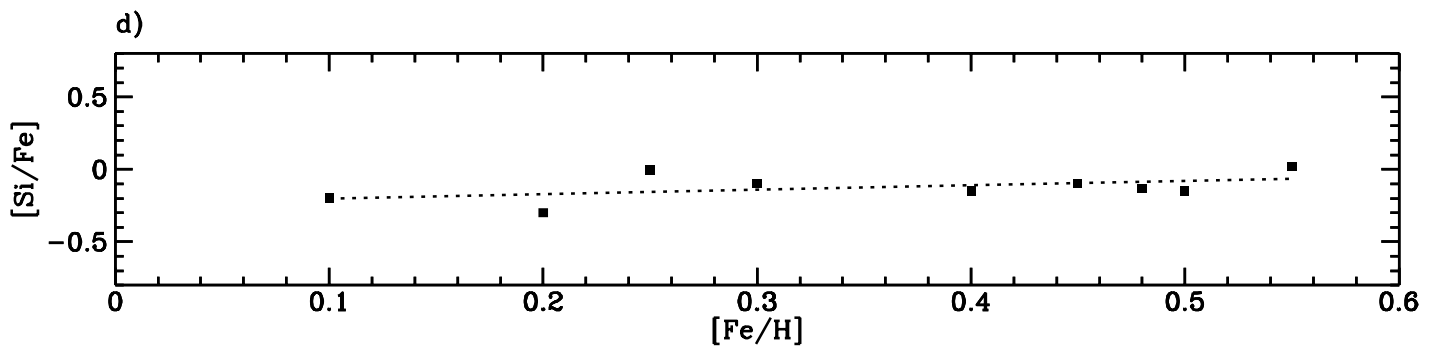
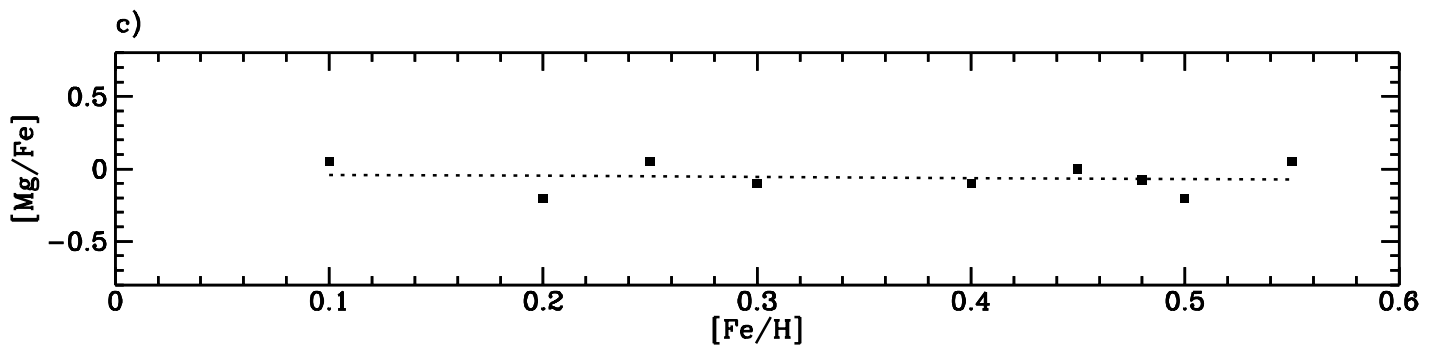
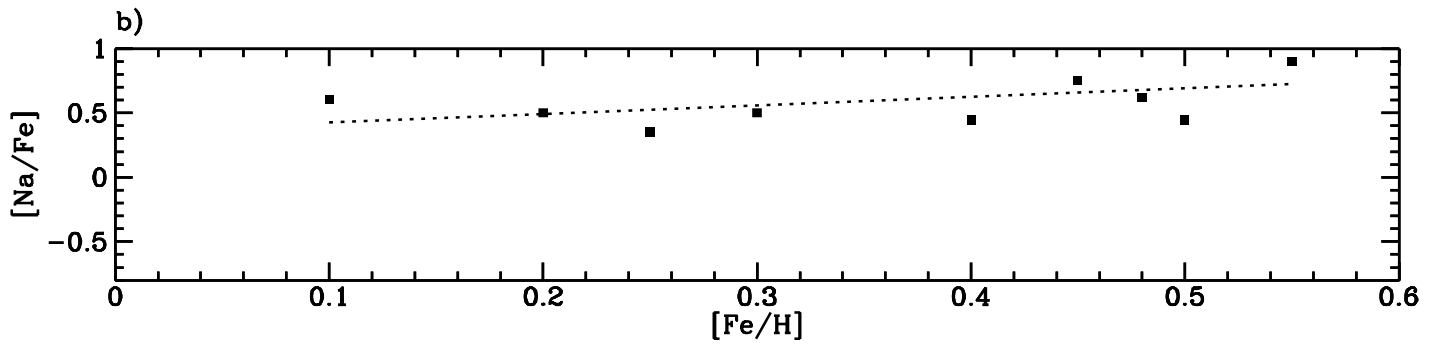
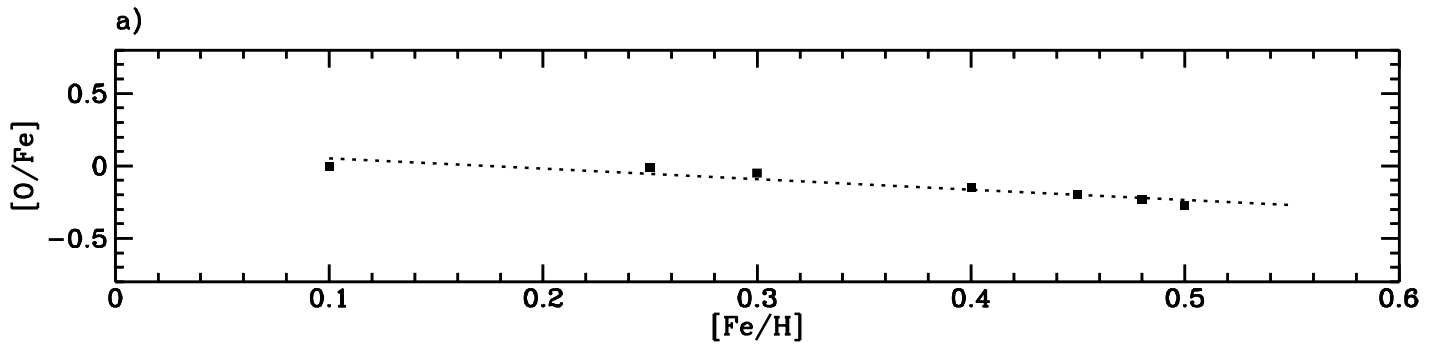


TABLE 3. ATMOSPHERE PARAMETERS

star	Geneva			adopted			
	T_{eff}	$\log g$	[Fe/H]	T_{eff}	$\log g$	[Fe/H]	ξ (km.s $^{-1}$)
BD + 9°1617	5137	4.54	+0.33	5200	4.30	+0.25	1.1
BD - 10°3166	5300	4.51	+0.56	5400	4.40	+0.50	1.0
BD - 11°4126	4800	4.61	+0.38	5000	4.30	+0.20	1.1
G161 - 29	4869	4.59	+0.42	5100	4.30	+0.10	1.0
G60 - 06	5052	4.56	+0.36	5300	4.60	+0.30	1.0
HD 99109	5202	4.53	+0.45	5400	4.20	+0.45	1.1
HD 115589	5221	4.53	+0.44	5400	4.54	+0.40	1.0
HD 126614	5368	4.50	+0.47	5500	4.20	+0.55	1.0
HD 138776	5510	4.21	+0.34	5700	4.20	+0.48	1.1

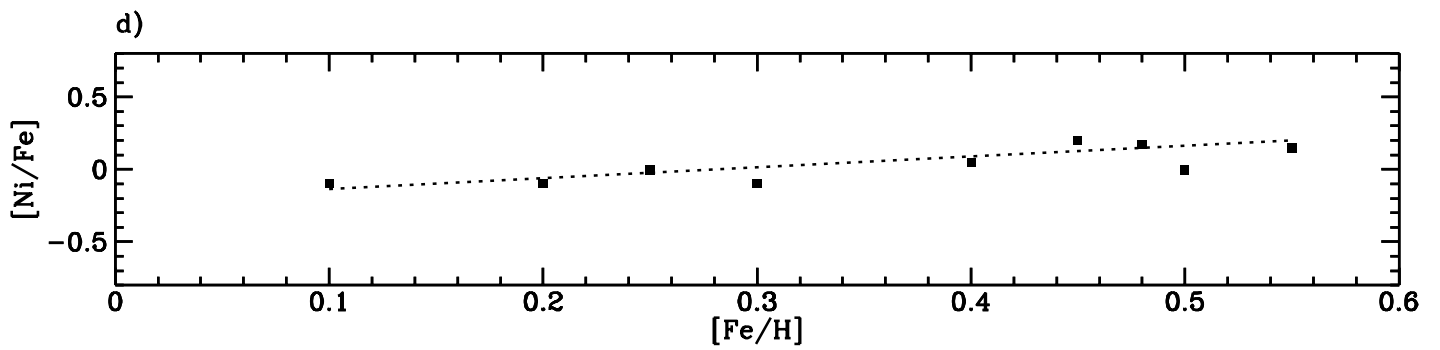
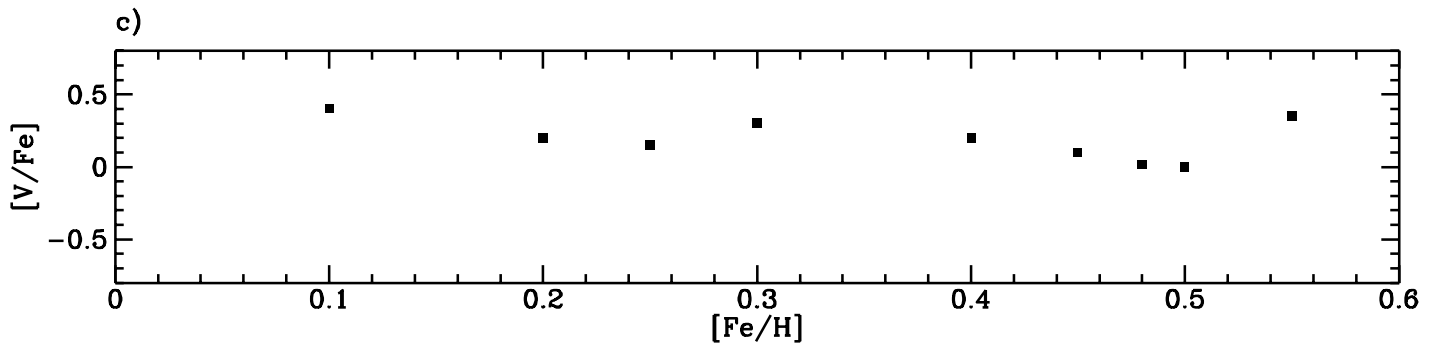
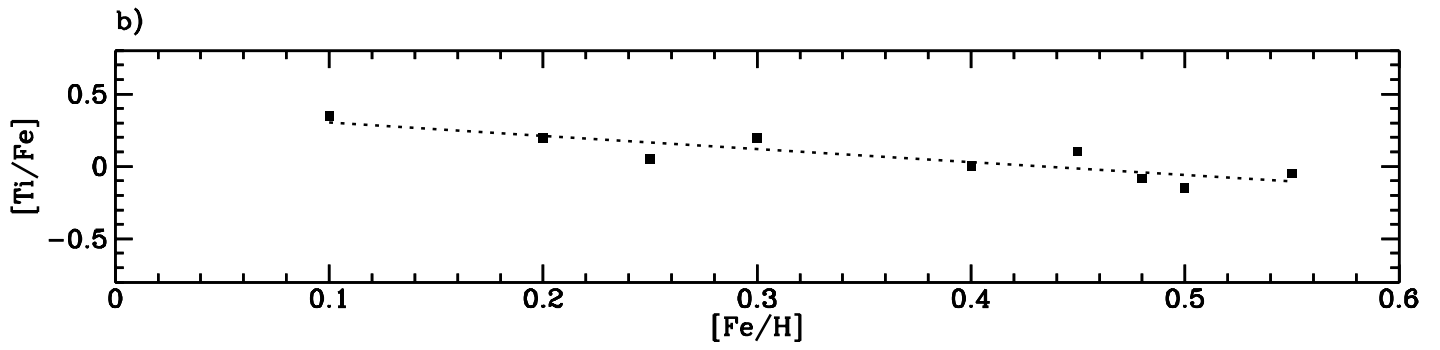
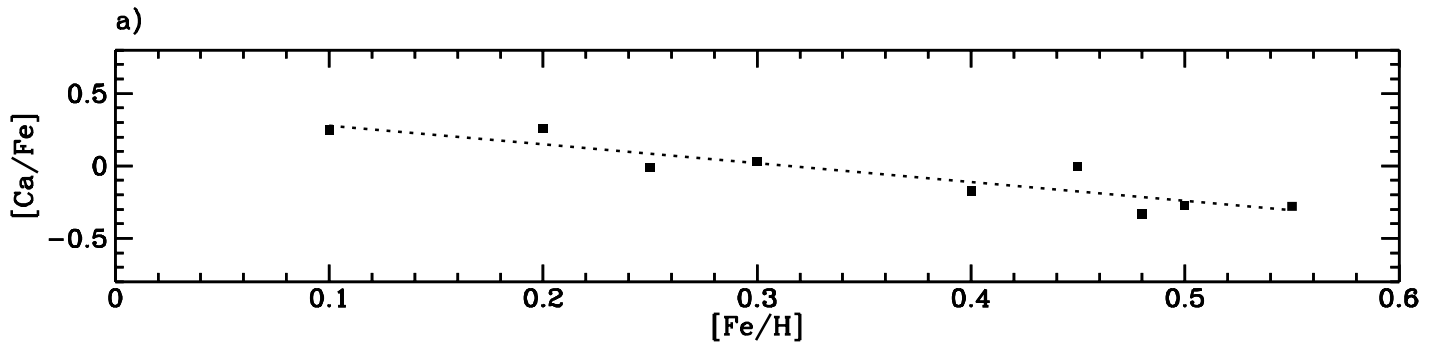


TABLE 4. ABUNDANCE RATIOS

star	[Na/Fe]	[Mg/Fe]	[Si/Fe]	[Ca/Fe]	[Ti/Fe]	[V/Fe]	[Ni/Fe]	[Zr/Fe]	[Y/Fe]	[Ba/Fe]	[Eu/Fe]
BD + 9°1617	+0.35	+0.05	0.00	-0.01	+0.05	+0.15	0.00	-0.38	-0.20	-0.23	...
BD - 10°3166	+0.45	-0.20	-0.15	-0.27	-0.15	0.00	0.00	...	-0.30	-0.50	-0.10
BD - 11°4126	+0.50	-0.20	-0.30	+0.26	+0.20	+0.20	-0.10	-0.65	-0.10	-0.03	+0.10
G161 - 29	+0.60	+0.05	-0.20	+0.25	+0.35	+0.40	-0.10	-0.40	+0.05	-0.30	+0.50
G60 - 6	+0.50	-0.10	-0.10	+0.03	+0.20	+0.30	-0.10	-0.27	-0.15	-0.40	+0.10
HD 99109	+0.75	0.00	-0.10	0.00	+0.10	+0.10	+0.20	-0.25	-0.15	-0.50	-0.10
HD 115589	+0.45	-0.10	-0.15	-0.17	0.00	+0.20	+0.05	-0.20	-0.22	-0.30	+0.10
HD 126614	+0.90	+0.05	+0.02	-0.28	-0.05	+0.35	+0.15	-0.40	...
HD 138776	+0.62	-0.08	-0.13	-0.33	-0.08	+0.02	+0.17	-0.42	...

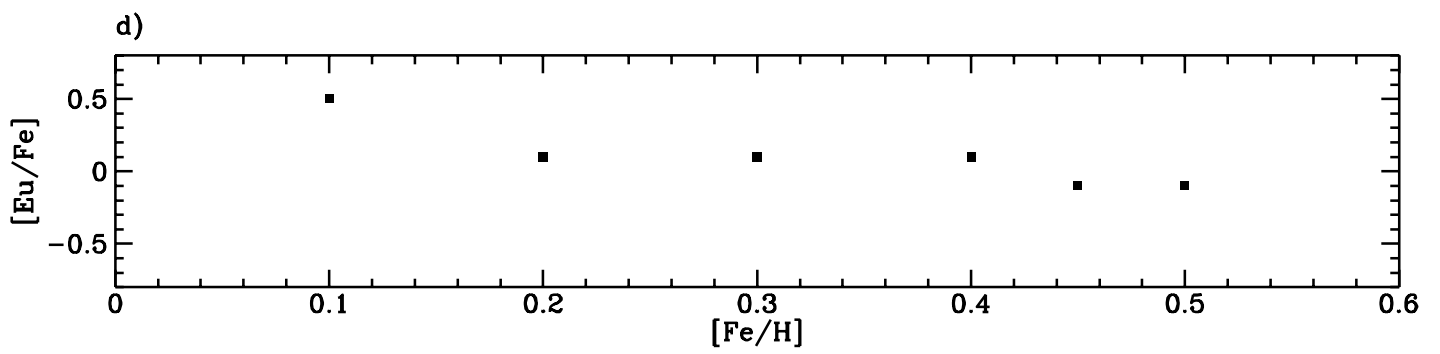
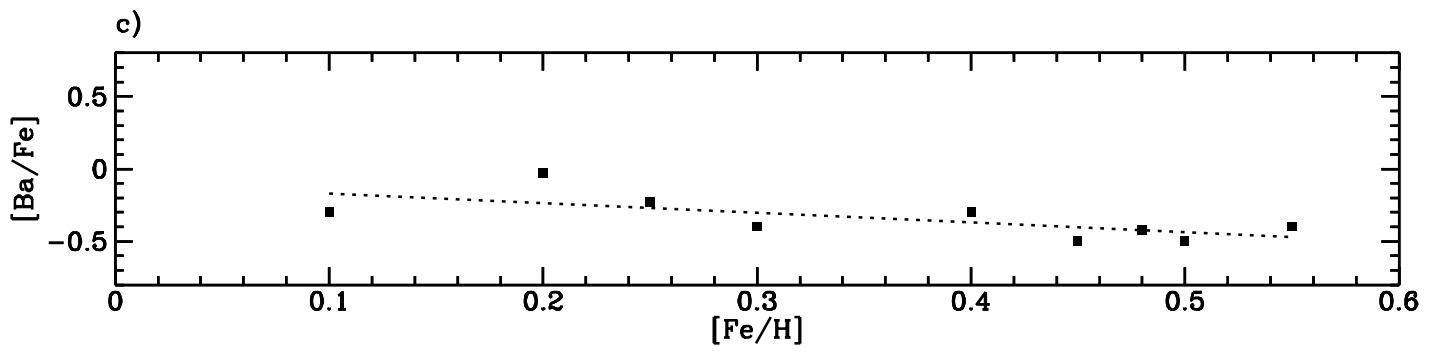
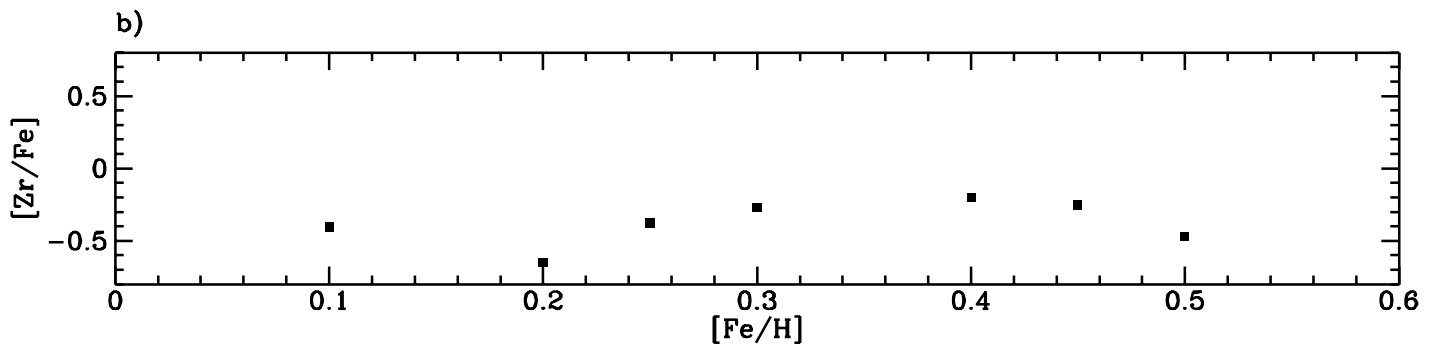
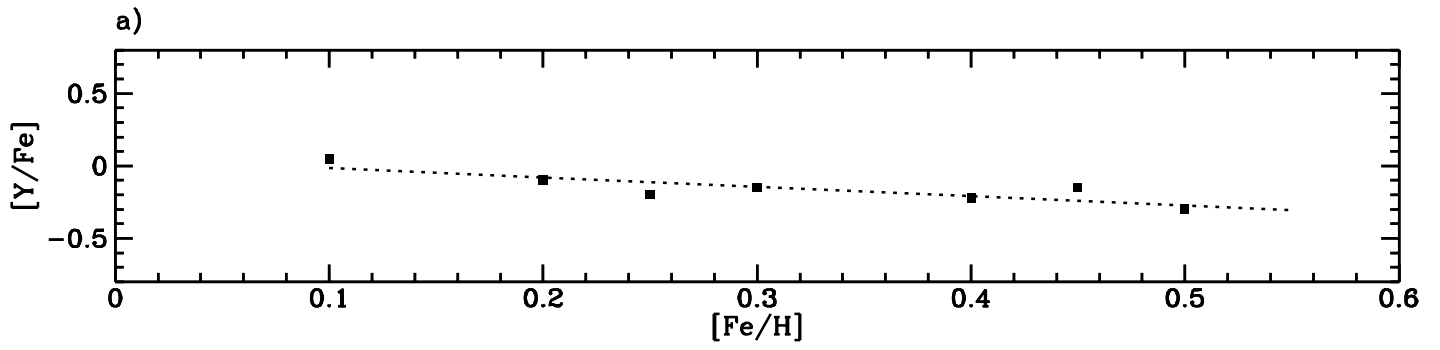
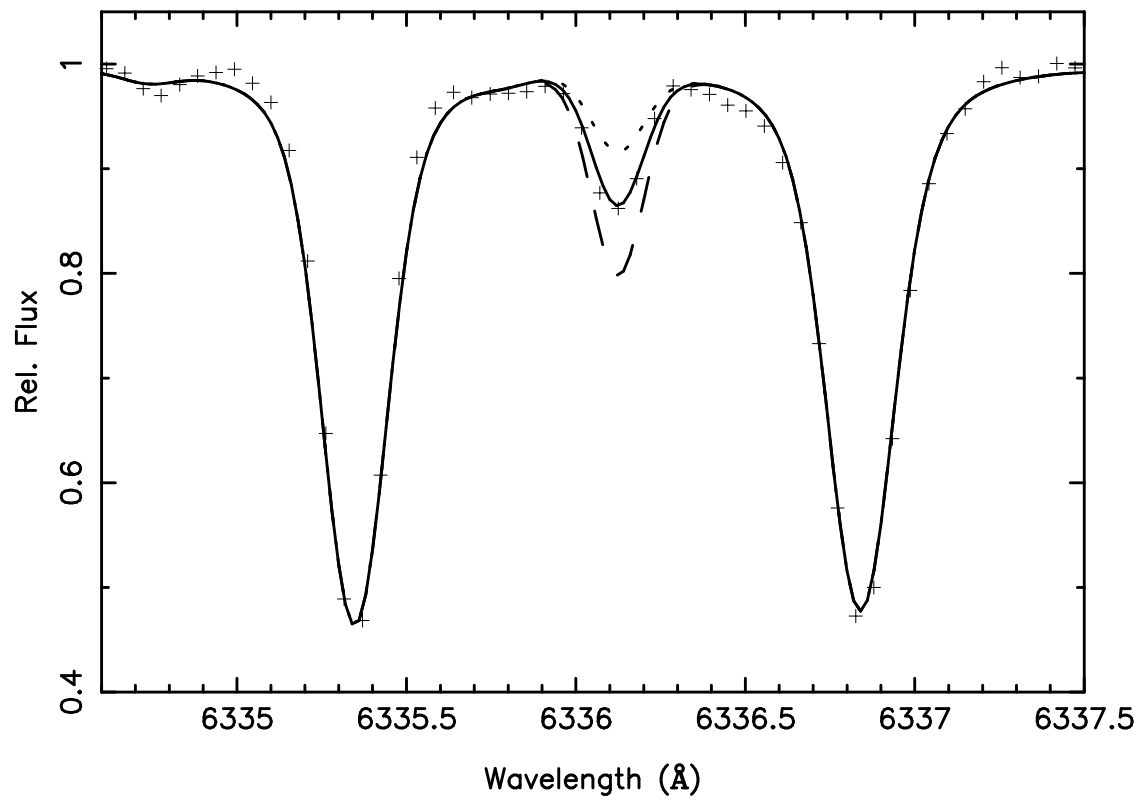
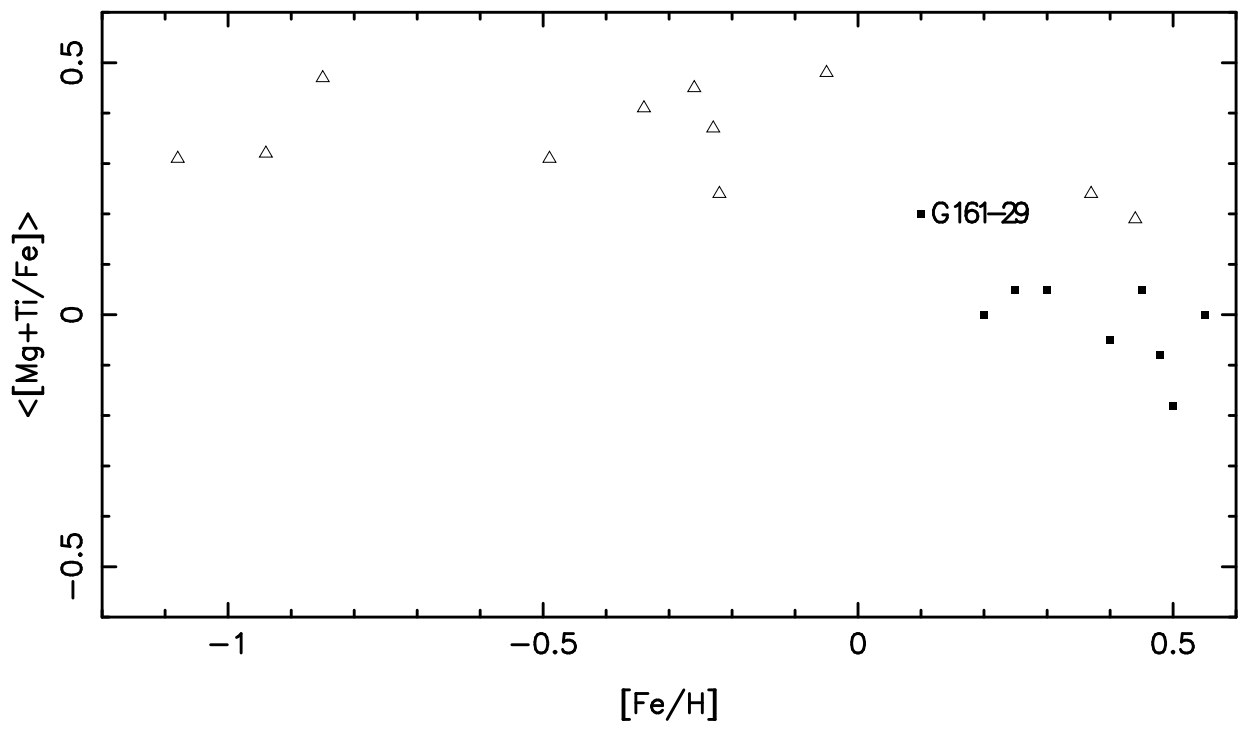
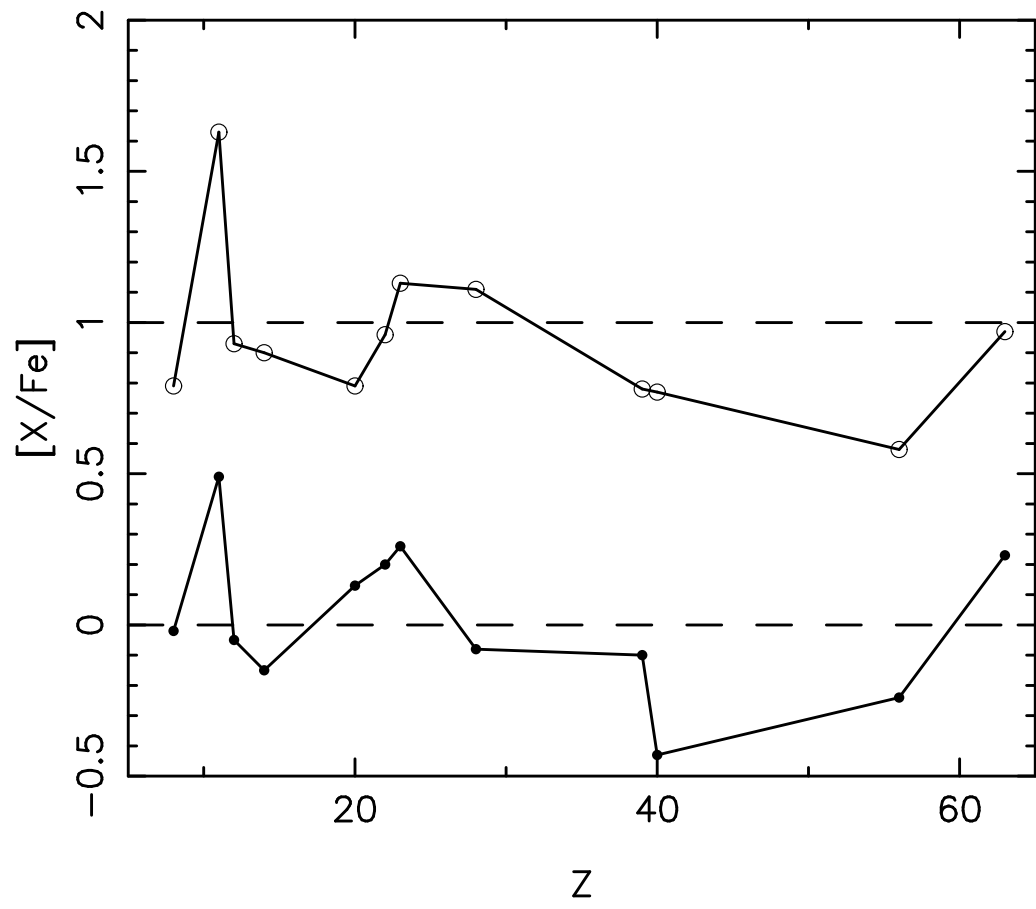


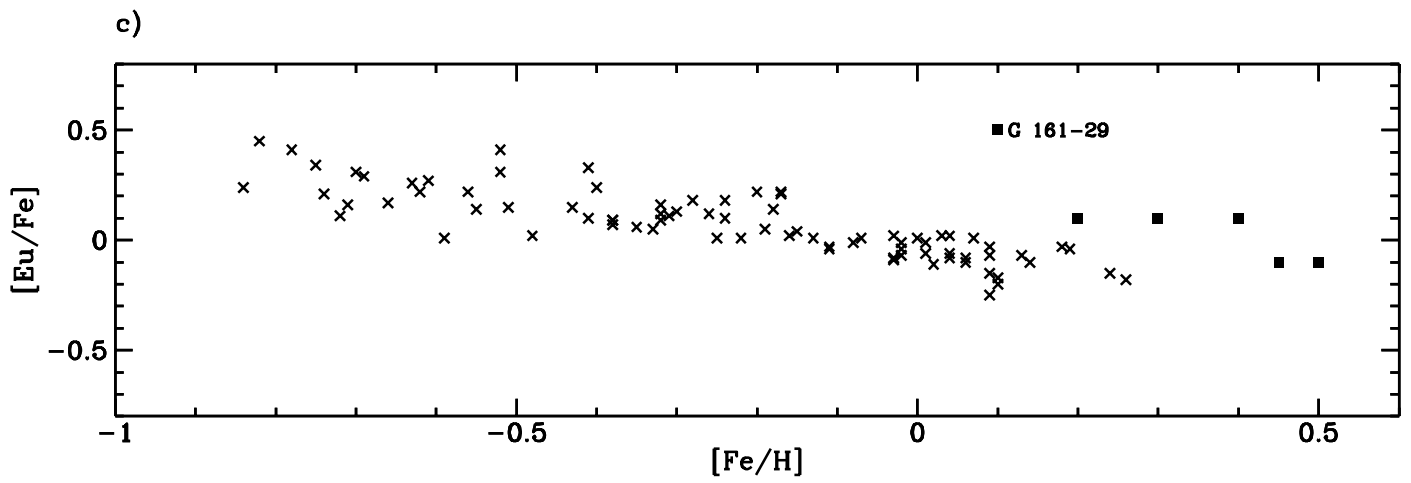
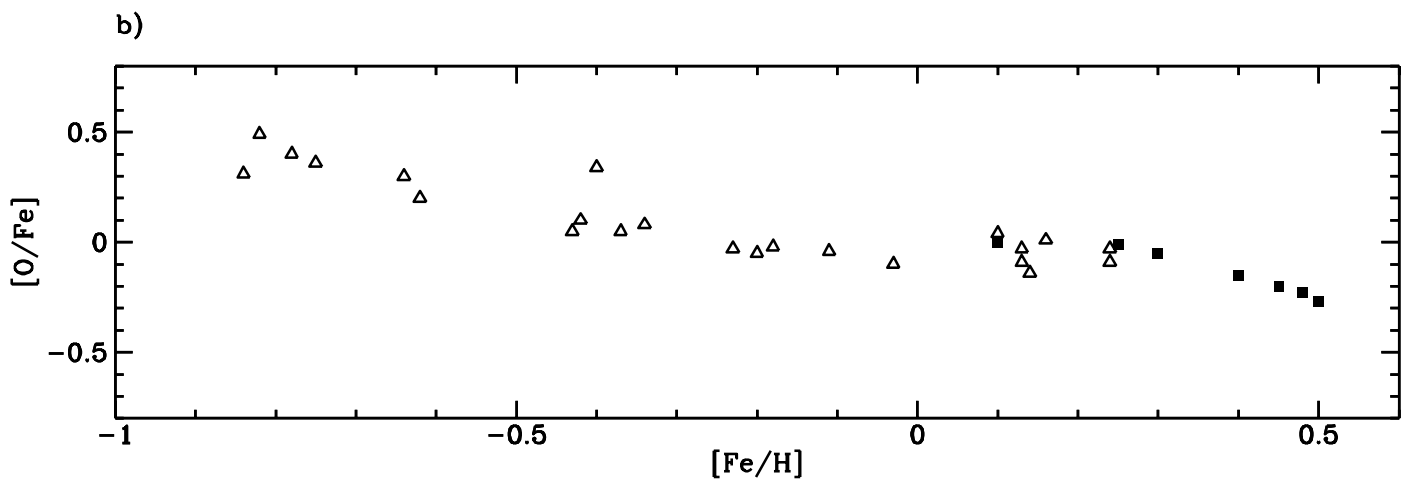
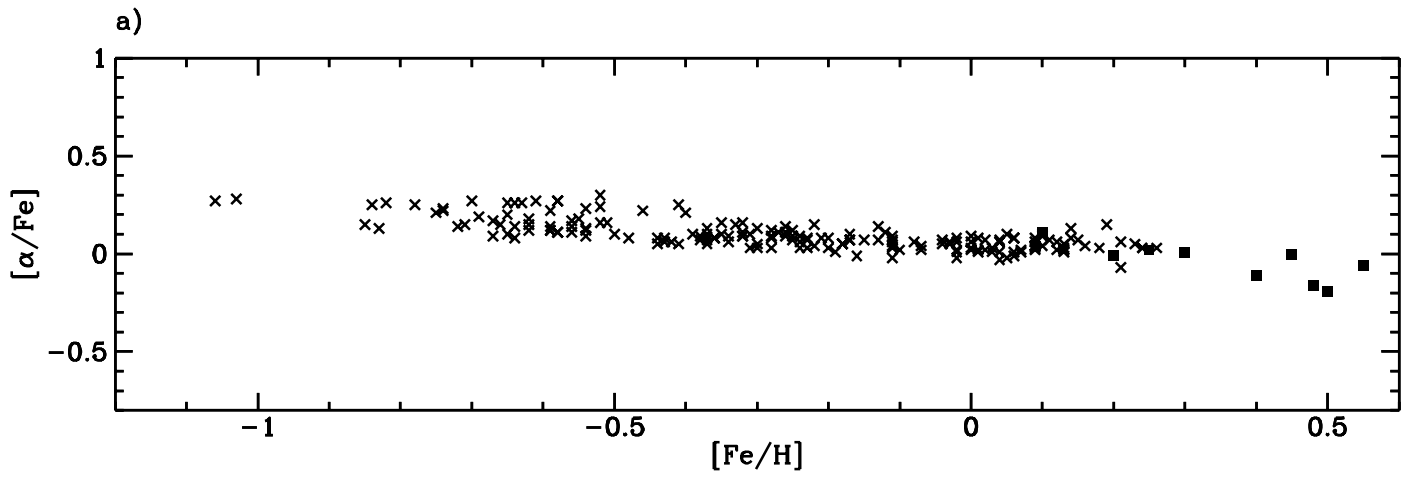
TABLE 5. OXYGEN ABUNDANCES RELATIVE TO IRON.

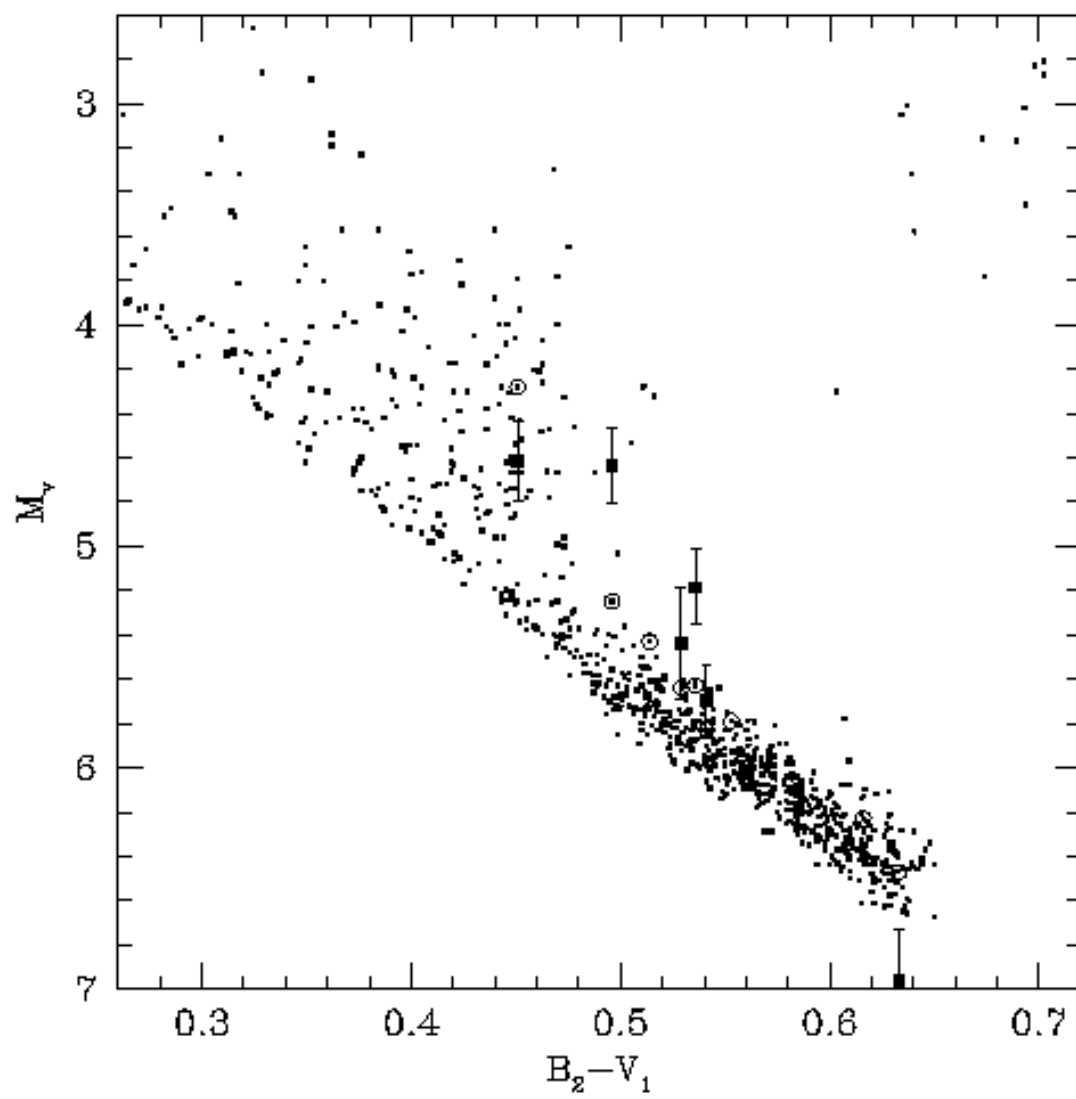
star	[O/Fe]		
	[C/H]=-0.2	[C/H]=0.0	[C/H]=+0.2
BD + 9°1617	-0.14	-0.01	-0.01
BD - 10°3166	-0.37	-0.27	-0.25
BD - 11°4126
G161 - 29	-0.08	0.00	+0.01
G60 - 6	-0.05	-0.05	0.00
HD 99109	-0.22	-0.20	-0.18
HD 115589	-0.21	-0.15	-0.15
HD 126614
HD 138776	-0.25	-0.23	-0.23











HIGH-RESOLUTION ABUNDANCE ANALYSIS OF VERY METAL-RICH STARS IN THE SOLAR NEIGHBORHOOD ¹

SANDRA CASTRO

Instituto Astronômico e Geofísico, CP 9638 São Paulo, SP 01065-970, Brazil, and Dept. of Astronomy, Columbia University, 538 W. 120th St., New York, NY 10027

R. MICHAEL RICH

Department of Astronomy, Columbia University, 538 W. 120th St., New York, NY 10027

M. GRENON

Observatoire de Genève, Chemin des Maillettes 51, CH-1290 Sauverny, Switzerland

B. BARBUY

Instituto Astronômico e Geofísico, CP 9638 São Paulo, SP 01065-970, Brazil

and

J. K. McCARTHY

Dept. of Astronomy, Caltech, MS 105-24, Pasadena, CA 91125

Received _____; accepted _____

¹ Observations collected at the McDonald Observatory, Texas, USA

ABSTRACT

We report detailed analysis of high-resolution spectra of nine high velocity metal-rich dwarfs in the solar neighborhood, selected from the proper motion samples of Grenon. The stars are super metal-rich, and 5 of them have $[\text{Fe}/\text{H}] \geq +0.4$, making them the most metal-rich stars currently known.

We find that α -elements decrease with increasing metallicity; s-elements are underabundant by about $[\text{s-elements}/\text{Fe}] \approx -0.3$; the Eu II line was measurable for 6 stars, showing $[\text{Eu}/\text{Fe}] \approx 0.0$, except for G161-29 where $[\text{Eu}/\text{Fe}] = +0.50$.

All calculations followed the same methods used by Castro *et al.* (1996) [AJ, 111, 2439] for the analysis of the well-known metal-rich prototype μ Leo and the very strong-lined bulge star BW IV-167, for which $[\text{Fe}/\text{H}] = +0.46$ and $+0.47$ were found respectively.

While exceeding the $[\text{Fe}/\text{H}]$ of current bulge samples, the chemistry of these stars has important similarities and differences. The near-solar abundances of the alpha-capture elements places these stars on the metal-rich extension of McWilliam & Rich (1994) [ApJS, 91, 749], but their s-process abundances are much lower than those of the bulge giants. These low s-process values have been interpreted as the hallmark of an ancient stellar population. We are unable to convincingly assign these stars to a known Galactic population and we urge further studies of larger samples.

1. Introduction

The Galaxy contains a number of little studied old, metal-rich stellar populations. In the canonical view of chemical evolution, metals slowly built up in the interstellar medium over time, and the youngest disk stars should be more metal-rich than the Sun. However, the actual metal-rich populations are instead *older* than 10 Gyr, particularly the field population of the Galactic bulge, and the bulge globular clusters (Ortolani *et al.* 1995). One may add to this list the metal-rich old open clusters in the disk (Phelps & Janes 1996), and disk dwarfs and giants in the Solar vicinity. While there are heuristic explanations for early enrichment in the Galactic center region, it is more difficult to explain the early formation of old metal-rich star clusters and local field stars away from the Galactic center. Yet high metallicities are found in these stars, and it is interesting to speculate that they may be related to the Galactic center in some way. On the other hand, these data may be telling us that high abundances could be reached in disk regions of relatively lower density, more distant from the Galactic Center.

About 4% of local disk stars are super metal-rich (defined as more metal-rich than the Hyades of $[\text{Fe}/\text{H}]=+0.12$), with metallicities estimated from Geneva photometry in the range $+0.30 < [\text{Fe}/\text{H}] < +0.60$. They are either the ultimate stage of the local disk chemical evolution or genuine members of the Galactic bulge, now scattered out in the disk.

The most metal-rich stars analyzed in the literature are found in the samples of Edvardsson *et al.* (1993), Luck & Challener (1995), Feltzing (1995) (hereafter F95) for the disk, McWilliam & Rich (1994) (hereafter MR94) and Castro *et al.* (1996) for the bulge.

Detailed compositions have also been determined for large numbers of local disk stars, some of which also have high metallicity. Edvardsson *et al.* (1993) analyzed a sample of 189 F and G disk stars in the range $-1.06 < [\text{Fe}/\text{H}] < +0.26$. F95 extended Edvardsson *et al.*'s sample by analyzing 50 disk metal-rich stars of metallicities in the range $-0.08 < [\text{Fe}/\text{H}] <$

+0.42. Luck & Challener (1995) analyzed 55 F/G field giants in the metallicity range of $-0.34 < [\text{Fe}/\text{H}] < +0.39$.

MR94 found that 11 Galactic bulge K giants in the metallicity range of $-1.08 < [\text{Fe}/\text{H}] < +0.44$ show enhancement of some α -elements such as Mg and Ti relative to Fe, but not in others such as Ca and Si. The MR94 giants also had Solar [s-process/Fe] ratios. Sadler, Terndrup & Rich (1996) found $[\text{Mg}/\text{Fe}] \approx +0.30$ for a sample of 400 K and M giant stars in the Baade Window. Idiart, Freitas Pacheco & Costa (1996) analyzed the integrated spectrum of the Baade Window and found $[\text{Mg}/\text{Fe}] = +0.45$ and $[\text{Fe}/\text{H}] = -0.02$, characterizing the bulge population mix. Castro *et al.* (1996) obtained $[\text{Fe}/\text{H}] = +0.46$ for μ Leo, considered the most metal-rich disk star, and $+0.47$ for BW IV-167, a strong lined star discovered by Rich (1988) and the most metal-rich star in the MR94 sample.

In this work we carry out detailed analysis of a sample of very metal-rich stars selected on the basis of their kinematics (perigalactica ≈ 3 kpc) and photometry (high metallicities). The most straightforward expectation is that $[\alpha\text{-elements}/\text{Fe}] > 0$ would be found if these stars formed from rapidly enriched gas (bulge-like history), whereas $[\alpha\text{-elements}/\text{Fe}] \approx 0$ if they are metal-rich disk stars (Edvardsson *et al.* 1993; F95). In reality, the even the MR94 bulge giants do not fit into this pattern, and we may not be able to definitively classify these stars as either bulge or disk. There is the additional possibility that these stars originate from a different stellar population altogether.

All calculations were carried out with the same methods employed in the analysis of the metal-rich disk star μ Leo by Castro *et al.* (1996), so that our results can be scaled to this prototype and extensively studied star.

In Sect. 2 the observations are described. In Sect. 3 the detailed analysis is reported. In Sect. 4 the discussion and conclusions are presented.

2. Observations

High-resolution spectra were obtained at the 2.1 m Struve telescope of the McDonald Observatory, using the Sandiford échelle spectrograph at the Cassegrain focus (McCarthy *et al.* 1993). A two-pixel resolution of $R = 60000$ was obtained with a 1.2 arcsec slit width, covering the wavelength region $\lambda\lambda$ 6000-7780 Å, contained in 30 orders. The slit length was 6.0 arcsec to prevent overlapping orders at the long wavelength limit. The reductions were carried out by using IRAF. The échelle data were extracted using an optimal background extraction routine (Tomaney & McCarthy 1996). The log-book of observations is reported in Table 1 and a typical spectrum is shown in Fig. 1. The signal-to-noise (S/N) values reported in Table 1 are each a mean of several spectral orders.

3. Detailed Analysis

The spectrum synthesis code used assumes Local Thermodynamic Equilibrium (LTE) and is described in Cayrel *et al.* (1991). The line list includes molecules of CN $A^2\Pi - X^2\Sigma$, $C_2 A^3\Pi - X^3\Pi$ and TiO $A^3\Phi - X^3\Delta$ (see Barbuy *et al.* 1991; Milone *et al.* 1991). Curves-of-growth were computed using the code RENOIR by M. Spite.

For all calculations, the model atmospheres by Kurucz (1992) were employed, where interpolations were made for the stellar parameters of our sample stars.

The equivalent widths of the lines were measured using the IRAF package and are reported in Tables 2a and 2b, together with excitation potential χ_{ex} and oscillator strengths $\log gf$. The $\log gf$ values of Fe I lines were adopted from Nave *et al.* (1994), while $\log gf$ values for elements other than Fe were taken from several sources and most of them were then fitted to the solar spectrum, as described in Castro *et al.* (1995). Sources for $\log gf$ values of elements other than Fe are listed in Table 2b. The selected Fe I lines were chosen

by discarding those showing known blends. In principle, most of the Fe I lines are clean of blends.

The continuum adopted for the measurement of equivalent widths is very close to the observed continuum and we did not attempt to place a higher continuum to take into account blanketing effects. An example of the continuum placement is given in Fig. 1.

3.1. Temperatures

The effective temperatures derived based on the Geneva photometry, given in Table 3, were checked through excitation equilibrium of Fe I lines. A mean difference of 150 K above the values derived from the Geneva photometry were found, as also noticed by Cayrel de Strobel (1996). In Fig. 2a, the curve-of-growth of Fe I for HD 138776 shows the good agreement between the lines of different excitation potential. Such temperatures were further checked using the $H\alpha$ line profile which confirmed the excitation equilibrium value. The $H\alpha$ profiles were computed using a revised version of the code HYDRO by Praderie (1967). In Fig. 2b is shown the fit of the computed $H\alpha$ wings to the observed profile for HD 138776. The final adopted temperatures are reported in Table 3.

3.2. Gravities

The gravities were derived through ionization equilibrium of Fe I and Fe II lines. The values so derived were found to be within 0.18 dex of the gravities predicted by the Geneva photometry. An average of 10 Fe II lines were available (Table 2b), which makes the gravity determination reliable.

3.3. Metallicities

The metallicities were calculated using Fe I lines with $W < 150 \text{ m}\text{\AA}$, in order to avoid saturation effects. Using all those Fe I lines as given in Table 2a, the metallicity derivation was carried out by comparing the theoretical curve of growth to that for the measured equivalent widths (Fig. 2a). The final metallicities are given in Table 3.

We also tested contamination by CN lines adopting a list selected by MR94 of CN-free Fe I lines, but changes in metallicities for the sample stars are negligible; we emphasize that the effect of CN contamination is more important in giant stars of low temperatures and high metallicities. However, our data are 3 times the resolution of MR94 and are generally higher S/N as well, making Fe lines in our data much less likely to have been blended with CN.

For most stars the resulting $[\text{Fe}/\text{H}]$ are in close agreement with the values predicted by the Geneva photometry. The results for BD-10°3166, HD 99109, HD 115589, HD 126614 and HD 138776 are among the most metal-rich values known. For example, in an analysis of 50 metal-rich stars of the Galactic disk, F95 obtained $[\text{Fe}/\text{H}] \approx 0.40$ for the most metal-rich ones of her sample.

Another interesting result is a comparison of our results to those for μ Leo, considered the most metal-rich disk star, and BW IV-167, one of the strongest-lined stars in the Rich (1988) sample: for these stars Castro *et al.* (1996) obtained $[\text{Fe}/\text{H}] = +0.46$ and $+0.47$ respectively, using the same analysis procedures employed in the present work.

3.4. Microturbulent Velocities

The microturbulent velocities were derived from the curves of growth which best fitted the weak lines and the flat portion of the curves at the same time. The microturbulent

velocities derived for the sample stars are listed in Table 3.

3.5. Relative Abundances

Table 4 gives the abundance ratios for analyzed elements relative to iron, as discussed below. Figures 3a through 3d show the results for O, Na, Mg, Si; Figures 4a through 4d give the results for Ca, Ti, V, Ni and Figures 5a through 5d show the abundance pattern for Y, Zr, Ba and Eu in the sample stars. The linear fits of [element/Fe] vs. [Fe/H] are indicated in the figures.

Sodium-to-Iron: [Na/Fe] ratio is enhanced and increases with increasing metallicity in agreement with F95. This would suggest an additional source of Na enrichment in the Galaxy such as synthesis of Na in the hydrogen burning shell of intermediate mass stars (Timmes, Woosley & Weaver 1995).

Oxygen: we have fitted synthetic spectra of the forbidden line [OI] at $\lambda 6300.311 \text{ \AA}$ by taking into account CO association. Since we do not dispose of carbon lines, we assume [C/Fe]=−0.2, 0.0 and +0.2; the resulting oxygen abundance is not much affected by the carbon abundance in these hot stars, as indicated in Table 5. We found that oxygen follows the trend of [O/Fe] ratio in the disk: oxygen abundances in our sample of stars declines from the solar value towards the most metal-rich stars and reaches [O/Fe]=−0.23, following the behavior of data by Nissen & Edvardsson (1992). Our stars seem to be the upper limit of [Fe/H] in their scale.

α -elements Mg, Si: Spectrum synthesis of the Mg I line at $\lambda 6319.242 \text{ \AA}$ was employed to derive Mg abundances. The Si I line at $\lambda 6721.84$ used to derive silicon abundances is a reliable abundance indicator as claimed by Gratton & Sneden (1990) (note that MR94 found this feature to be blended and to give spuriously high abundances in metal-rich stars,

less of a concern at our resolution). Mg and Si relative to Fe are approximately constant with metallicity. The average of Mg abundance for our sample is about ≈ -0.06 and [Si/Fe] slightly increases with increasing metallicity.

α -elements Ca, Ti: calcium and titanium are essentially solar to subsolar relative to Fe. Abundances derived from Ca I lines at $\lambda 6166.440$, $\lambda 6455.605$, $\lambda 6508.846$ Å and Ti I line at $\lambda 6336.113$ Å show a slight decline as metallicity increases, the same result found by Edvardsson *et al.* (1993). The Ti I line used for spectrum synthesis is shown in Fig. 6 for HD 115589. It is a weak and the most reliable line of our list (the same was observed by MR94).

Iron-peak-elements V, Ni: vanadium and nickel behave in different ways. V is overabundant with a mean value of +0.2 dex, but may be affected by hyperfine splitting. Ni shows a slight increase towards the more metal-rich stars and both results are in good agreement with the work by Porto de Mello (1996) who analyzed the abundance distribution of solar-type stars in the solar neighborhood.

r-process-element Eu: europium was available for 6 sample stars. The solar ratio is found for Eu in 5 stars, and G 161-29 shows [Eu/Fe]=+0.5. This result for G 161-29 would imply that Supernovae Type II would have had importance in the chemical enrichment of its original gas (Meyer 1994). This star will be discussed at the end of this section.

s-process-elements Y, Zr, Ba: We have found that Y, Zr and Ba are underabundant relative to iron. Y and Ba tend to decrease to subsolar values as metallicity increases, again in agreement with F95 and Porto de Mello (1996). On the other hand, Zr is subsolar in all sample stars in disagreement with most stars of F95’s sample but compatible with her values for the coolest stars. The two entries for the Ba II line in Table 2b are hyperfine components of a same line as described by François (1996).

The s-process abundances are clearly different from the sample of MR94 and we discuss the issue further in Sec. 4. Further study of the s-process elements in both these disk stars and Galactic bulge giants is very important.

G161-29 seems to be different from the other sample stars. It shows high europium, titanium and calcium, but low magnesium and oxygen abundances relative to iron: $[\text{Eu}/\text{Fe}] = +0.5$, $[\text{Ti}/\text{Fe}] = +0.35$, $[\text{Ca}/\text{Fe}] = +0.2$, $[\text{Mg}/\text{Fe}] = +0.05$ and $[\text{O}/\text{Fe}] = +0.0$. In fact, this star might belong to the bulge population, showing similarities to the MR94 results, where some α -elements showed to be overabundant but not all of them. In Figure 7 is shown $([\text{Mg}/\text{Fe}] + [\text{Ti}/\text{Fe}])/2$ for the MR94 bulge stars and our sample, where it can be seen that G161-29 fits the bulge pattern. It is also interesting to notice that G161-29 might be very similar to the stars in the sample of Barbuy & Grenon (1990) which show kinematic and photometric properties of possible bulge members.

3.6. Uncertainties

We explore the effect of the following changes in input parameters: $\Delta T_{\text{eff}} = \pm 100$ K, $\Delta \log g = \pm 0.1 \text{ cm.s}^{-2}$, $\Delta \xi = \pm 0.4 \text{ km.s}^{-1}$ and $\Delta W = \pm 15 \text{ m}\text{\AA}$. The dependence of metallicity on T_{eff} and $\log g$ is nearly negligible and is ± 0.05 . On the other hand, the variation of metallicity with microturbulent velocity is $\Delta[\text{Fe}/\text{H}] = -0.10$ dex as we apply the change $\Delta \xi = +0.40 \text{ km.s}^{-1}$.

The abundance ratio uncertainty has a random component which arises from equivalent width measurement and is typically $\Delta[\text{Fe}/\text{H}] \approx 0.10$ dex. For an element X represented by several lines, the random component of the uncertainty is diminished by the square root of the number of lines. The typical mean uncertainty of our equivalent width measurement is about $10 \text{ m}\text{\AA}$. We estimate a final uncertainty of about ± 0.2 in elemental ratios $[\text{X}/\text{H}]$.

4. Conclusions

We have acquired high-resolution, high S/N spectra of 9 G-K dwarf stars in the solar neighborhood, kinematically and photometrically selected by M. Grenon. We have used curve of growth and spectrum synthesis calculations to derive abundances for these stars. We conclude that 5 of these stars are now the most metal-rich stars with a high-resolution abundance analysis.

The abundance pattern of our sample stars, illustrated in Fig. 8 where the elemental ratios $[X/Fe]$ are plotted vs. the atomic number Z , is characterized by:

(i) Sodium-to-iron ratio is overabundant for all stars where this element was available.

(ii) There is a decrease of the α -elements-to-iron (O, Ca, Ti) with increasing metallicity, as illustrated in Fig. 9a which compares the mean α -element abundance given in Table 12 of Edvardsson *et al.* (1993), and the mean value of our determination for Mg, Si, Ca and Ti. Another interesting comparison is given in Fig. 9b which shows the $[O/Fe]$ data of Nissen & Edvardsson (1992)'s stars plotted with our data.

(iii) Europium-to-iron ratio is about solar for all stars except for G161-29 (notice that this star also shows enhancement of Ti and Ca). It is interesting to compare the $[Eu/Fe]$ ratio for our 5 disk stars to the results obtained by Woolf, Tomkin & Lambert (1995). The trend of decreasing $[Eu/Fe]$ with increasing metallicity shown by their data is not confirmed by the $[Eu/Fe] \approx 0.0$ of our sample stars as given in Fig. 9c.

(iv) s-process elements are underabundant relative to iron.

In comparison to MR94, the most striking difference is that the s-process elements are subsolar here, which was not the case in MR94. We note that $[Ba/Fe]$ in particular can be used as a crude chronometer (Edvardsson *et al.* 1993) such that the lower $[Ba/Fe]$, the older the stars. A straightforward application leads us to conclude that these stars must be

older than those of MR94. On the other hand, the clearly established tendency for $[O/Fe]$ to continue declining at high metallicities argues for a substantial contamination by Type I SNe; i.e., the population formed over so long a timescale that the slower Type I SNe could be the dominant source of metals.

In principle, the decrease of O, Ca, Ti, Y and Ba relative to Fe with increasing metallicity could also be explained by infall of material processed in halo Supernovae Type I, as suggested by Freitas Pacheco (1993). However this is contradicted by the high $[Mg/Fe] \approx 0$ and $[Si/Fe] \approx 0$ in the metallicity range of our sample, which shows that a more complex scenario is necessary to explain the chemical enrichment of the most metal-rich disk stars.

4.1. The Nature of these Stars

Are our stars members of the local disk, interlopers from the bulge, or an entirely new stellar population?

The location of our sample stars in the color-magnitude diagram M_V vs. $(B_2 - V_1)$ of the most metal-rich stars in the solar neighborhood within 120 pc is shown in Fig. 10. The absolute magnitudes of our sample stars derived from the Geneva photometry and those derived from the Hipparcos parallaxes are indicated by circles and filled squares respectively. Our sample stars define a locus of an evolved main-sequence composed of the most metal-rich stars. We first consider the possibility that these stars are the final stages of the evolution of the disk. If this is the case, their high eccentricity orbits and chemistry support their ancient nature, and one might speculate that these stars represent the final generation of the inner disk population.

Rose (1985) identified a class of strong-lined dwarf stars in the Galactic disk using

a gravity-independent metal-abundance index. This index indicated that the stars were strong-lined in their Fe lines and in general they appeared to be as strong-lined as the most metal-rich stars in the Cayrel de Strobel & Bantolila (1983) $[\text{Fe}/\text{H}]$ catalog, i.e., those stars with published $[\text{Fe}/\text{H}] > +0.25$.

Boulade, Rose & Vigroux (1988) found that the three strong-lined G dwarfs of their sample (which includes HD 126614 with $[\text{Fe}/\text{H}]$ given by Grenon), had near UV indices that clearly established them to be more strong-lined than solar-abundance stars. They hence concluded that although there was no detailed abundance analysis carried out for those unusual G dwarfs at that time, their strong-lined nature was evident in a variety of spectral indices.

Membership in the Galactic bar is attractive, but these data do not provide a confirmation. Since a bar dominates the central kpc, it is possible that some stars on chaotic orbits manage to diffuse out of, or are ejected from, the bar population. Thus the local Grenon stars would be these members of the bar that were ejected.

The similarity to the MR94 sample is tantalizing (Figure 7) but not complete. As their metallicity increases, the composition of the MR94 bulge giants tends toward Solar; this is also true of the s-process elements. While the α -element patterns look very similar to the metal-rich bulge giants of MR94, the clearly subsolar s-process abundances are a problem and make the bulge origin look much less likely. Because they are produced in the envelopes of AGB stars, s-process elements are likely enhanced on a longer timescale than that of the Fe-peak elements produced in Type I SNe (and more easily distributed in the ISM).

The final possibility is that the stars originate in a new stellar population, perhaps the older, central regions of the disk. While the deep potential well of the Galactic center would appear to be the logical place for stars to reach high metallicities, it appears that this process has occurred in surprising places such as old Galactic clusters. It is conceivable that

the early disk was able to reach very high local abundances even at large galactocentric radii. We are led to conflicting interpretations: ancient origins from the s-process, color-magnitude diagram, and enhanced alpha-elements, yet an extended formation history and Type I SN enrichment based on the decline of $[O/Fe]$ to subsolar values in the most metal-rich stars.

While the nature of these peculiar stars remains uncertain, there is a clear need for a larger sample of these high-velocity, metal-rich stars.

We are grateful to Greg Langmead for the data reduction. SC acknowledges the Fapesp PhD fellowship n^o 92/1351-3 and the CNPq fellowship n^o 201703/93-9. We acknowledge useful discussions with Andy McWilliam, James Truran, and George Wallerstein.

REFERENCES

- Barbuy, B., & Grenon, M. 1990, in *Bulges of Galaxies*, eds. B. J. Jarvis & D. Terndrup, ESO Conf. Workshop Proc. 35, p.83
- Barbuy, B., Spite, F., Spite, & M., Milone, A. 1991, A&A 247, 15
- Biémont, E., Karner, C., Meyer, G., Traeger, F., & zu Putlitz, G. 1982, A&A 107, 166
- Boulade, O., Rose, J. A., & Vigroux, L. 1988, AJ, 96, 1319
- Castro, S., Barbuy, B., Bica, B., Ortolani, S., & Renzini, A. 1995, A&AS 111, 17
- Castro, S., Rich, R. M., McWilliam, A., Ho, L. C., Spinrad, H., Filippenko, A. V., & Bell, R. A. 1996, AJ 111, 2439
- Cayrel, R., Perrin, M. -N., Barbuy, B., & Buser, R. 1991, A&A 247, 108
- Cayrel de Strobel, G., Bentolila, C. 1983, A&A 119, 1
- Cayrel de Strobel, G. 1996, A&ARv. 7, 243
- Edvardsson, B., Gustafsson, B., Nissen, P. E., Anderssen, J., Lambert, D. L., & Tomkin, J. 1993, A&A 275, 101
- Feltzing, S. 1995, PhD thesis, University of Uppsala
- François, P. 1996, A&A 313, 229
- Freitas Pacheco, J. A. 1993, ApJ 403, 673
- Fuhr, J. R., Martin, G. A., & Wiese, W. L. 1988, J. Phys. Chem. Ref. Data, Vol. 17, No. 4
- Gratton, R. G., & Sneden, C. 1990, A&A 234, 366
- Grenon, M. 1989, ASSci 156, 29
- Idiart, T., Freitas Pacheco, J. A., & Costa, R. D. D. 1996, AJ 111, 1169
- Kurucz, R. 1992, in *The Stellar Populations of Galaxies*, eds. B. Barbuy & A. Renzini (Dordrecht: Kluwer), 225

- Luck, R. E., & Challener, S. L. 1995, AJ 110, 2968
- Martin, G. A., Fuhr, J. R., & Wiese, W. L. 1988, J. Phys. Chem. Ref. Data, Vol. 17, No. 3
- McCarthy, J. K., Sandiford, B. A., David, B., & Booth, J. 1993, PASP 105, 881
- McWilliam, A. 1990, ApJS 74, 1075
- McWilliam, A., & Rich, R. M. 1994, ApJS 91, 749
- Meyer, B. S. 1994, ARA&A 32, 153
- Milone, A., Barbuy, B., Spite, M., & Spite, F. 1991, A&A 261, 551
- Moore, C. E., Minnaert, M. G. J., & Houtgast, J. 1966, The Solar Spectrum, 2935 Å to 8770 Å (NBS Monog. 61; Washington, DC:NBS)
- Nave, G., Johansson, S., Learner, R. C. M., Thorne, A. P., & Brault, J. W. 1994, ApJSS 94, 221
- Nissen, P. E., & Edvardsson, B. 1992, A&A 261, 255
- Ortolani, S., Renzini, a., Gilmozzi, R., Marconi, G., Barbuy, B., Bica, E., & Rich, R. M. 1995, Natur 377, 701
- Phelps, R. L., & Janes, K. A. 1996, AJ 111, 1604
- Porto de Mello, G. 1996, in *Stellar Abundances*, eds. B. Barbuy, W. Maciel & J. Gregorio-Hetem (IAG-USP: Brazil), 59
- Praderie, F. 1967, Ann. Phys. 30, 31
- Rich, R. M. 1988, AJ 20, 828
- Rose, J. A. 1985, AJ 90, 803
- Sadler, E. M., Terndrup, D. M. & Rich, R. M. 1996, AJ 112, 117
- Smith, G. 1981, A&A 103, 351
- Spite, M., Barbuy, B., & Spite, F. 1989, A&A 222, 35

Timmes, F. X., Woosley, S. E., & Weaver, T. A. 1995, *ApJS* 98, 617

Tomaney, A. B., & McCarthy, J. K. 1996, in preparation

Wolf, V. M., Tomkin, J., & Lambert, D. L. 1995, *ApJ* 453, 660

FIGURE CAPTIONS

Fig. 1.— HD 99109: a typical spectrum showing the high S/N ratio and the local continuum.

Fig. 2.— (a) Curve-of-growth of Fe I for HD 138776, illustrating the agreement between lines of different excitation potential. (b) H α line in HD 138776: observed spectrum (solid line) and synthetic spectra computed for $T_{\text{eff}} = 5500$ K (dotted line) and 5700 K (dashed line) which represents the best fit.

Fig. 3.— Abundance ratios vs. [Fe/H] for our sample stars for: (a) [O/Fe]; (b) [Na/Fe]; (c) [Mg/Fe]; (d) [Si/Fe]. Linear fits [element/Fe] vs. [Fe/H] are indicated in the diagrams.

Fig. 4.— Abundance ratios vs. [Fe/H] for our sample stars for: (a) [Ca/Fe]; (b) [Ti/Fe]; (c) [V/Fe]; (d) [Ni/Fe]. Linear fits [element/Fe] vs. [Fe/H] are indicated in the diagrams.

Fig. 5.— Abundance ratios vs. [Fe/H] for our sample stars for: (a) [Y/Fe]; (b) [Zr/Fe]; (c) [Ba/Fe]; (d) [Eu/Fe]. Linear fits [element/Fe] vs. [Fe/H] are indicated in the diagrams.

Fig. 6.— Synthetic spectrum of the Ti I line at $\lambda 6336.113$ Å for HD 115589. The lines represent the synthetic spectra calculated with [Ti/Fe] = -0.3 (dotted), 0.0 (solid), $+0.3$ (dashed) and the observed spectrum (crosses).

Fig. 7.— $[\alpha/\text{Fe}]$ vs. [Fe/H] for McWilliam & Rich (1994) bulge stars (triangles) and the sample stars (squares) where only Mg and Ti are taken into account.
 $\langle \text{Mg} + \text{Ti} \rangle = \frac{1}{2}([\frac{\text{Mg}}{\text{Fe}}] + [\frac{\text{Ti}}{\text{Fe}}])$

Fig. 8.— Element ratios relative to iron [X/Fe] for the sample stars vs. the atomic number Z: upper points (shifted by a constant equal to 1.0 in [X/Fe]) correspond to the 5 stars with [Fe/H] ≥ 0.40 (open circles) and lower points refer to the 4 stars with [Fe/H] ≤ 0.30 (filled circles).

Fig. 9.— (a) $[\alpha/\text{Fe}]$ vs. $[\text{Fe}/\text{H}]$ for the sample stars (squares) compared to those from Edvardsson *et al.* (1993) (x), where $[\alpha/\text{Fe}] = \frac{1}{4}([\text{Mg}/\text{Fe}] + [\text{Si}/\text{Fe}] + [\text{Ca}/\text{Fe}] + [\text{Ti}/\text{Fe}])$; (b) $[\text{O}/\text{Fe}]$ vs. $[\text{Fe}/\text{H}]$ for our sample stars (squares) compared to those from Nissen & Edvardsson (1992) (triangles); (c) $[\text{Eu}/\text{Fe}]$ vs. $[\text{Fe}/\text{H}]$ for our sample stars (squares) compared to those from Woolf, Tomkin & Lambert (1995) (x).

Fig. 10.— Color-magnitude diagram of our sample stars plotted together with solar neighborhood main sequence stars. The absolute magnitudes are derived from the Geneva photometry (circles) and from the Hipparcos parallaxes (filled squares).